MARITIME TRANSPORTATION RESEARCH AND EDUCATION CENTER
TIER 1 UNIVERSITY TRANSPORTATION CENTER
U.S. DEPARTMENT OF TRANSPORTATION

Large Scale Evaluation of Erosion Resistance of Biocementation against Bridge Scour and Roadway Shoulder Erosion

01/20/2018 – 03/20/2019

Lin Li
Yadong Li
Shihui Liu (GRA)

Dept. of Civil & Environmental Engineering
Jackson State University
Jackson, Mississippi

Final Report Date: 04/01/2019

FINAL RESEARCH REPORT
Prepared for:
Maritime Transportation Research and Education Center

University of Arkansas
4190 Bell Engineering Center
Fayetteville, AR 72701
479-575-6021

ACKNOWLEDGEMENT
This material is based upon work supported by the U.S. Department of Transportation under Grant Award Number 69A3551747130. The work was conducted through the Maritime Transportation Research and Education Center at the University of Arkansas.

1. Project Description

Soil is a living ecosystem where biogeochemical processes such as mineral precipitation, gas generation, biofilm formation and biopolymer generation are ubiquitous. Microbially induced calcite precipitation (MICP) is a sustainable method and a bio-geochemical process that induces calcium carbonate precipitation within the soil matrix as a consequence of microbial metabolic activity. MICP is one type of microbial geotechnical approaches for soil stabilization. It has recently gained much attention from geotechnical engineering researchers worldwide. The MICP naturally happens and is induced by nonpathogenic organisms that are native to the soil environment (DeJong et al., 2006). *Sporosarcina pasteurii* (ATCC 11859) has been widely used for MICP due to its highly active urease enzyme, which catalyzes the reaction network towards precipitation of calcite (DeJong et al., 2006; Chou et al., 2011; Zhao et al., 2014; Jiang et al., 2016; Pham et al., 2016; Li et al., 2018; Bu et al., 2018ab; Wen et al., 2018ab). This urea hydrolysis process produces dissolved ammonium (NH_4^+) and inorganic carbonate (CO_3^{2-}). The released ammonia subsequently increases pH, leading to accumulation of insoluble $CaCO_3$ in a calcium rich environment (i.e., $CaCl_2$). The urea hydrolysis reactions are shown as below:

$$CO(NH_2)_2 + 2H_2O \rightarrow CO_3^{2-} + 2NH_4^+ \quad (1)$$

$$Ca^{2+} + CO_3^{2-} \rightarrow CaCO_3\downarrow \quad (2)$$

The precipitated $CaCO_3$ can be used as bio-mediated cohesive material to improve engineering properties of sandy soil.

When the flow-induced erosive force exceeds the resistive force of geological materials, surface erosion and scour occur around transportation infrastructure, such as roadway shoulder erosion and bridge scour. Heavy rain or flood water may erode the roadway shoulders, causing pavement drop-off which directly affects the health condition of the pavement and poses risks to the traveling public. Bridge scour can scoop out scour holes around bridge piers or abutments. As scour occurs progressively, supporting material of bridge foundations is removed and replaced with material that has little or no bearing capacity. Thus, scour can quickly reduce the load capacities of bridge foundations and is most common cause of bridge failure from floods. Around 60% of all bridge

failure cases were caused by local scour and other hydraulic related issues (Landers 1992). According to Hydraulic Engineering Circular No. 23 (Lagasse et al. 2009) and NCHRP reports 593 (Lagasse et al. 2007), there are two types of countermeasures for bridge scour: "actively" reducing the erosive force by altering the flow patterns and "passively" increasing the resistive force by armoring the riverbed. For example, Li and Tao (2015) proposed streamlining of the bridge pier as an option to actively reduce turbulence intensity in the local zone and thus to decrease overall local scour potential. Armoring countermeasures include rigid revetments, flexible revetments, articulating revetments and bed armor, vegetated riprap, or vegetated geosynthetics that have been widely used in engineering applications (Lagasse et al. 2009). The Mississippi Department of Transportation has recognized the need and value to improve the resistivity of bridge pier and roadway shoulder to water erosion. For example, under 2 funding support of MDOT, Zheng (2013) evaluated bring scour at the bridge substructures and their impact on the bridge safety across the Mississippi. Scour monitoring with sensors technology and scour prediction with numerical predications have been recommended. However, there is limited information about how to increase the resistive force by armoring the riverbed. This study explores an alternative approach for prevention of bridge scour and road shoulder erosion. This approach allows the geomaterials to be improved in-situ using the emerging sustainable ground improvement method: biocementation through microbial induced calcite precipitation (MICP).

In Bao et al. (2017), the effect of MICP on surface erosion of granular soils was studied. The treated soil samples were tested in a flume to investigate the erosional behavior; both surface erosion and bridge scour tests were conducted. It was found that, while the untreated soil is highly erodible, the erosion of the MICP-treated sand is negligible under the test situations; but some concerns are raised regarding to practical applications. Erosion reduction of coastal sand dunes using MICP has been studied by Shanahan and Montoya (2016) through laboratory wave tank experiments. Through the application of MICP cementation to unsaturated to partially saturated sand dunes, the wave action induced erosion is significantly reduced.

The feasibility of biocementation through MICP as a soil improvement technique has been demonstrated in the laboratory using sand column experiments (DeJong et al. 2010, Martinez et

al. 2013, Shanahan and Montoya 2016). Most studies on MICP soil improvement used acrylic cylindrical columns or syringes for samples preparation by pumping or injections methods. Although pumping or injections promoted cementation media penetrate into soil pores under pressure to some extent, the effluent also reduces the number of bacteria as well as a portion of urease produced by bacteria, and the samples may not be uniform along the flow. Besides the injection method, immersing (or soaking) method has been developed by (Zhao et al. 2014b). Full contact flexible geotextile molds are used for samples preparation to allow the specimen being fully immersed in cementation media. A much uniform MICP-treated sample can be prepared through this method. The immersing method has been used in Li et al. (2018) and Bao et al. (2017). The objective of this study is to induce biocementation through MICP to provide an alternative approach for soil improvement and for in-situ improved geomaterials to resist bridge scour and road shoulder erosion.

2. Methodological Approach

2.1 Materials

To produce MICP-treated samples, following materials were used in the experiments:

2.1.1 Sand

Ottawa silica sand (99.7% quartz) shown in Figure 2-1 was used in the experiments. The sand is uniformly with a median particle size of 0.46 mm and no fines were included. It was classified as poorly graded sand based on the Unified Soil Classified System.

(a) (b)

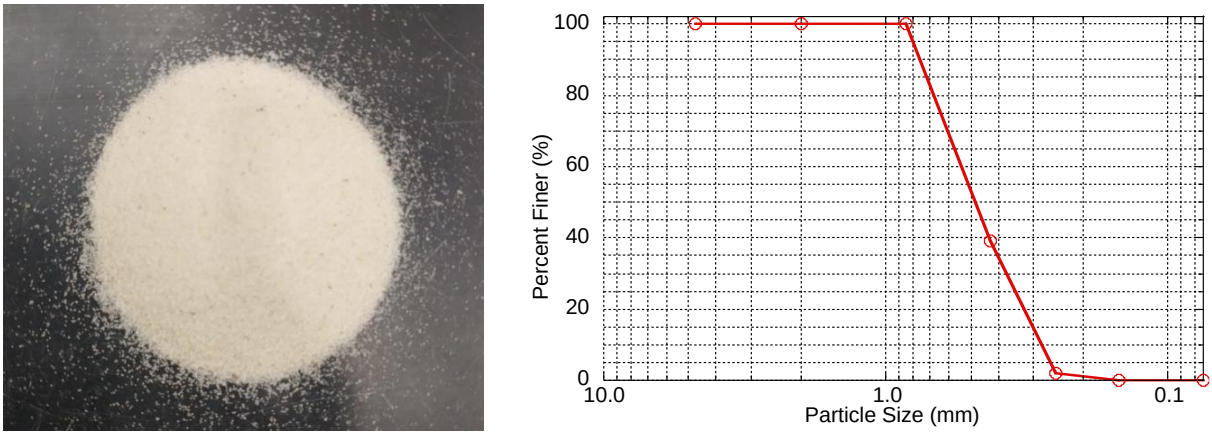

Figure 2-1. Ottawa silica sand used in the experiments

The Mississippi local sand shown in Figure 2-2 used in the experiments was obtained from Jackson, Hinds county, Mississippi. Its median particle size was 0.33 mm. It was classified as well graded fine sand in accordance with the Unified Soil Classification System.

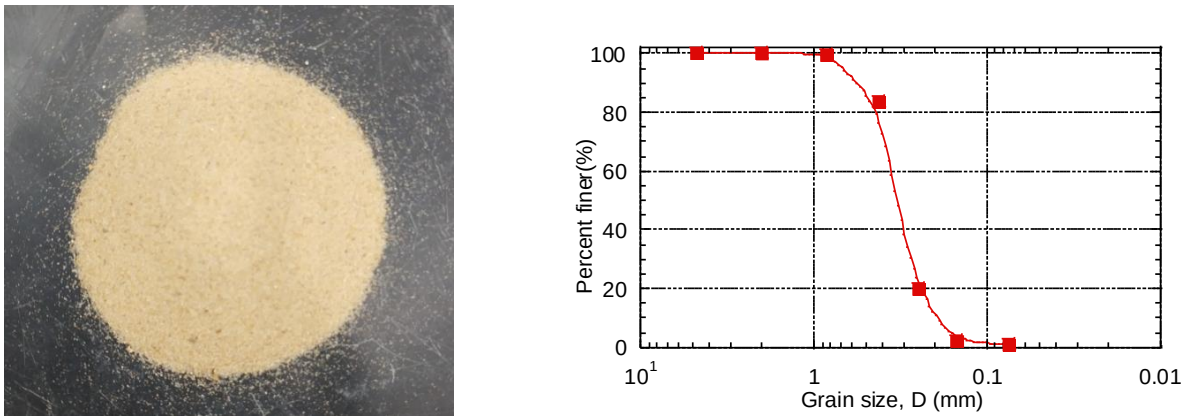

(a) (b)

Figure 2-2. Mississippi local sand used in the experiments

2.1.2 Bacteria and Cementation Media

S. pasteurii (ATCC 11859) shown in Figure 2-3 was used in the experiments. The bacteria were cultivated in ammonium-yeast extract media (growth media; ATCC 1376), which is constituted by following per liter of deionized water: (1) 0.13 M tris buffer (pH = 9.0), (2) 10 g $(NH_4)_2SO_4$, and (3) 20 g yeast extract. The bacteria and growth media were centrifuged at 4,000 g for 20 min after incubating aerobically at 30℃ in a shaker at 200 revolutions per min overnight. Then supernatant was removed and replaced with fresh growth media before the bacteria was re-suspended every time. The bacteria concentration was controlled by measuring absorbance (optical density) of the suspension using a spectrophotometer (Genesys 20, Thermo Scientific) at 600-nm wavelength. The concentration of bacteria cells suspended in the growth medium was calculated by the Eq. 3. The bacteria were grown for 24–28 h to an optical density (OD) of 600 nm (OD_{600}) of 0.3–1.5 (10^7–10^8 cells/mL; Qabany et al. 2012). The bacteria and growth media were stored in centrifuge vials at 4°C until used (Mortensen, Haber et al. 2011). The OD_{600} of bacteria solution in this study was fixed as 0.6.

$$Y=8.59 \times 10^7 \bullet Z^{1.3627} \quad (3)$$

where Z is reading at OD_{600}, and Y is the concentration of cells/mL (Ramachandran, Ramakrishnan et al. 2001).

Cementation media was used to provide chemical compositions for ureolysis, including urea, $CaCl_2$ $2H_2O$, NH_4Cl, $NaHCO_3$, and nutrient broth (Mortensen, Haber et al. 2011). The chemical concentration of cementation media in this study was 0.5M and 0.25M. The urea-Ca^{2+} molar ratio was 1: 1. For 0.5M chemical concentration, the chemical compositions were 10.0 g/L NH_4Cl, 3 g/L nutrient broth, 2.12 g/L $NaHCO_3$, 30 g/L urea, and 73.5 g/L $CaCl_2 \cdot 2H_2O$. For 0.25M chemical concentration, the chemical compositions were 10.0 g/L NH_4Cl, 3 g/L nutrient broth, 2.12 g/L $NaHCO_3$, 15 g/L urea, and 36.8 g/L $CaCl_2$ $2H_2O$. The pH of the cementation media was maintained as 6.0 at the beginning of the MICP process.

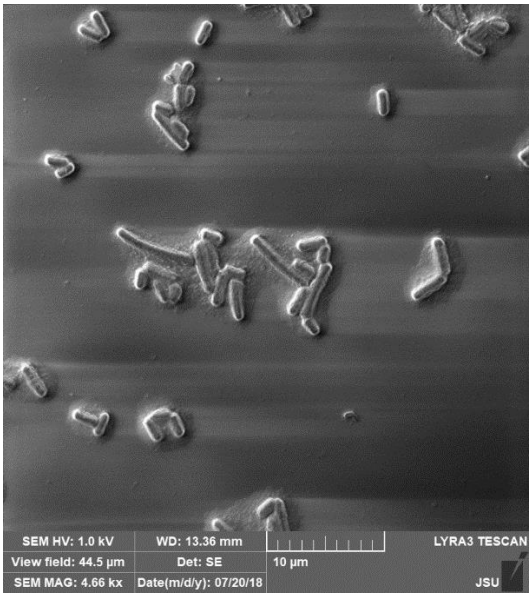

Figure 2-3. SEM image of *S. pasteurii*

2.1.3 Portland Cement

Portland cement (TYPE I/II, ASTM C150) was used as the cementing agent for the cement-treated samples. Its early strength gain allowed the various curing times ranged from 7 to 21 days. The specific gravity of cement grains is 3.15.

2.1.4 Full Contact Flexible Mold

The full contact flexible mold (FCFM) was developed by Zhao et al. (2014a). It was made by non-woven geotextile, which is a polypropylene, staple-fiber, needle-punched nonwoven material with grab tensile strength of 1700 kN; grab elongation of 50%, trapezoidal tear of 670 kN; apparent opening size of 0.15 mm; water flow rate of 34 mm/s; thickness of 1.51 mm, and unit mass of 200 g/m^2. The mold was fully permeable to cementation media. The size of unconfined compression test mold was 38.1 mm in diameter and 76.2 mm in height. The molds consisted of an annular part, a bottom and a cover as shown in Figure 2-4. Cylinder shape sample was prepared by FCFM to conduct UCS test.

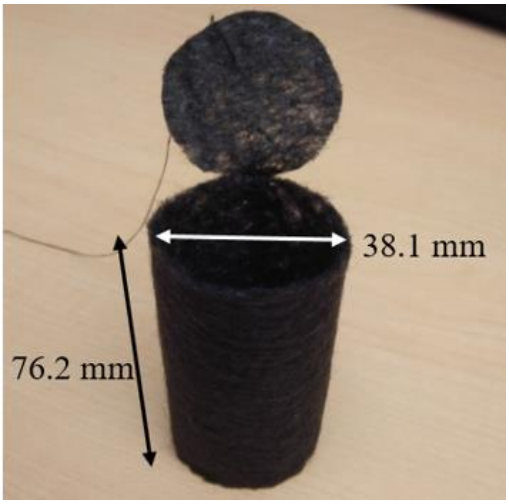

Figure 2-4. Photograph of full contact flexible mold for UCS test

2.1.5 Rigid Full Contact Mold

The rigid full contact mold (RFCM) includes flexible layer and rigid holder. The rigid holder was made by Polypropylene (PP) perforated sheet with 6.35 mm thickness. This PP sheet has 6.35 mm diameter tactic holes and the distance between holes is 9.53 mm. The rigid holder was assembled with different piece of PP sheet by long screw rod and nut. The holder size can be varied to meet different needs. As shown in Figure 2-5, the RFCM (a) was used for rainfall induced erosion test with dimension of 300 mm × 300 mm × 50 mm (L × W× H). Meanwhile, the RFCM (b) was used for brick compression strength test, four-point bending test, and accelerated erosion test. To prepare identical three specimens in one MICP treatment, the rigid holder included three chambers as shown in Figure 2-5(b). The size of each chamber was 177.8 mm in length, 76.2 mm in width and 38.1 mm in height.

(a)

(b)

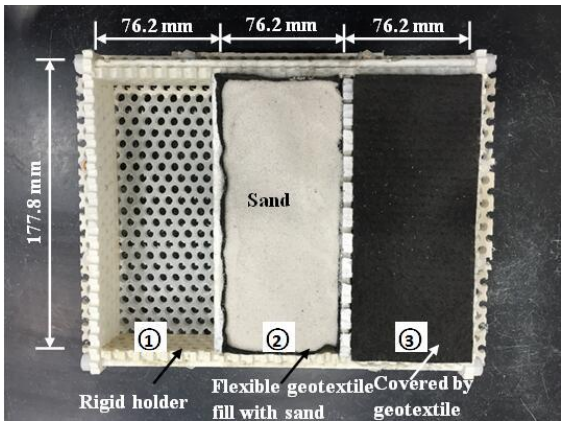

Figure 2-5. Photograph of RFCM of samples for rainfall induced erosion test (a) and RFCM of samples for compressive strength test, bending test, and accelerated erosion test (b)

The flexible layer of RFCM is made of geotextile. The geotextile is a polypropylene, staple fiber and needle punched nonwoven material, which has the same properties with geotextile for FCFM.

2.1.6 Fiber

Fibermesh 150e (FIBERMESH) shown in Figure 2-6 was used in this study to improve the ability for MICP-treated sand to resist accelerated water erosion. It is a 100% uniform homopolymer poly-propylene multifilament fiber with a specific gravity (Gs) of 0.91. It is chemically inert with high acid salt resistance. The length and thickness of the fibers used in this study are 12 mm and 0.1 mm, respectively, with an aspect ratio of 120 between the length and thickness of the fiber. Consoli

et al. (2009) used similar fibers of different lengths for the reinforcement of sand. It was concluded that fibers with an aspect ratio above 300 experienced strain hardening behavior, which caused significant mechanical problems such as fracture failures during shearing of the soil and a significant decrease in the ductility behavior of the fiber. The aspect ratio of the fiber used in this study was lower than the upper limit determined in the previous studies, indicating that it should provide efficient reinforcing performance (Consoli, Vendruscolo et al. 2009). In the fiber reinforcement, fiber content was fixed as 0.3% (by weight of dry sand), which was the optimum fiber content from Li et al. (2015).

Figure 2-6. Photograph of synthetic fibers used in this study

2.2 Samples preparation

2.2.1 MICP-treated Samples Preparation

All MICP-treated samples, either for rainfall induced erosion or for accelerated erosion, were prepared in tank reactors. The reactor shown in Figure 2-7 included a reactor tank containing soil samples, cementation media, sample supported shelf, and air pumps to provide oxygen for bacteria. A major feature of this method is to allow soil samples to fully immerse into the cementation media and to allow the cementation media to freely diffuse into the soil samples instead of using pump to inject cementation media.

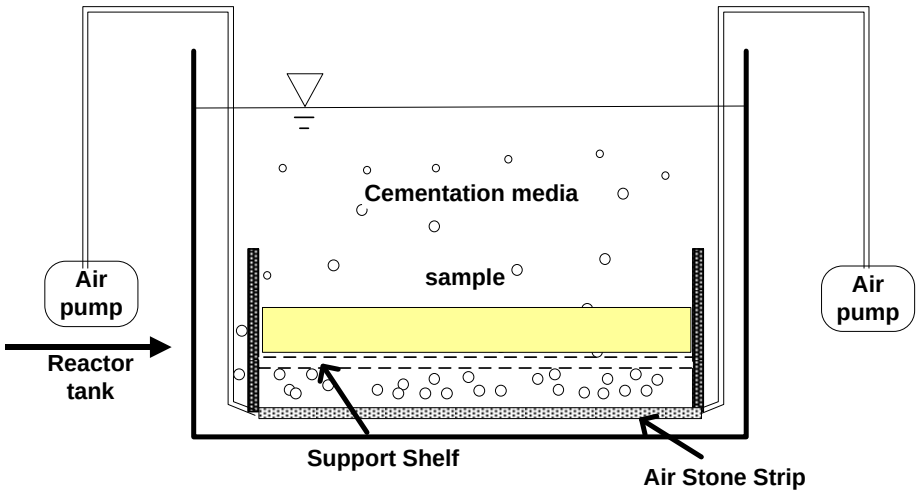

Figure 2-7. Sketch of Batch Reactor for MICP process

In the batch reactor, there is not hydraulic gradient to drive the flow through the soil samples. The hydraulic conductivity of the MICP-treated sand is in the range of 0.001 cm/s, which is permeable to cementation media. When the chemical of cementation media reacts under the catalysis of bacteria, the concentration of these chemicals is lower in the soil samples, which causes the chemical substances diffuse from high concentration area to low concentration area to continue the MICP process deeper in the soil samples.

As the cementation media permeates into the soil samples, MICP can occur in sample pores and the produced $CaCO_3$ can bond the sand particles together to improve the engineering properties. Many studies have used pump to inject cementation media into sample pores to promote the MICP process in samples. Using this method, the $CaCO_3$ content often varied in samples along the direction of the cementation media flow and even sometimes clogged the soil pore spaces near the injection point (Stocks-Fischer et al. 1999, Whiffin et al. 2007).

In the samples using RFCM for rainfall induced erosion tests, 8000 g sand was uniformly mixed with 2500-mL bacteria solution and then air pluviated into the mold to reach a median dense condition (D_r in the range of approximately 42–55%, and dry density of sand ranged from 1.58–

1.64 g/cm^3). In the samples using RFCM for accelerated erosion tests, 900 g sand was uniformly mixed with 200 mL bacteria solution and then air pluviated into the mold to reach the same condition as rainfall induced erosion samples. For fiber reinforced sample, the required 200 mL bacteria solution was first added into 900 g dry sand to prevent floating of the fibers in the soil matrix, and then the proposed content (0.3% by weight of dry sand in this study) of fibers was mixed in small increments by hand to obtain a uniform mixture. It is important to ensure that all fibers are mixed thoroughly (Shao et al. 2014). Then all the samples were placed on the shelf (shown in Figure 2-7) and then immerged the entire shelf into the batch reactor where was filled with cementation media. Following methods of Zhao et al. (2014a), the MICP process maintained for 7 days without adding any additional cementation media, bacteria, or growth media. The shelf and samples were removed from the reactor at the end of the reaction time. Then, the MICP-treated samples were removed from the molds by cutting the molds. The samples were oven dried for 48 h before being retreated or testing.

After the first MICP treatment, multiple MICP treatments developed by Wen et al. (2018b) may applied on the samples with following multiple treatments procedure if needed:

1) Oven dried the samples for 48 h;

2) Soak the samples into a fresh bacteria solution with OD_{600} of 0.6;

3) Replaced old cementation media with a new cementation media at the same concentration in the batch reactor;

4) Immersed the samples into batch reactor for another 7 days of reactions.

From step 1) to step 4) was MICP single treatment. Repeat step 1) to step 4) when more treatments are needed.

2.2.2 Cement-treated Samples Preparation

Cement-treated samples were prepared by mixing dry sand with type I/II cement. The proportion of added cement were 5% and 10% by weight of dry sand in this study. For preparation of rainfall

induced erosion sample, 8000 g dry sand was mixed with dry cement and 2500 mL water were added to achieve a uniform mixture which was similar to Bernadi et al. (2014). The cement-sand mixture was added into a rigid mold and cured for 7 days in a constant humidity of 100% and constant temperature of 25 ℃. The size of rigid mold was 300 mm in length, 300 mm in width and 50 mm in height. The accelerated erosion sample was prepared by the same method, 900 g dry sand was mixed with dry cement and 200 mL water were mixed uniformly and added into rigid mold as shown in Figure 2-8(a) and cured for 7 days in a constant humidity of 100% and constant temperature of 25 ℃. The size of rigid mold was 177.8 mm in length, 76.2 mm in width and 38.1 mm in height. In order to ensure a flat surface was achieved, a straightedge was used on the top of the samples upon completion of compaction. The samples were oven dried to dismiss the excess moisture after demolding (Figure 2-8(b)). Following testing or treatments were conducted on the samples after oven dried.

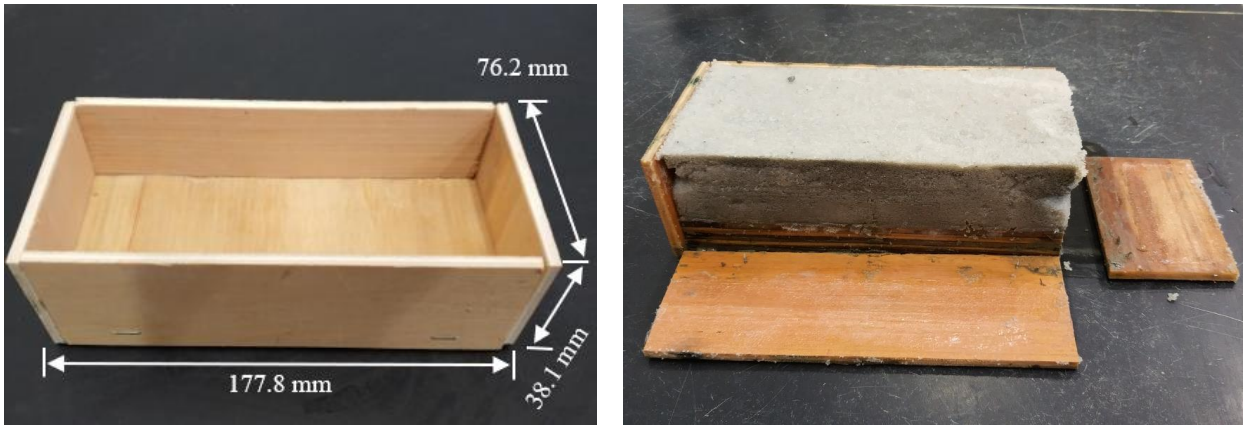

(a) (b)

Figure 2-8. Cement-treated sample preparation; (a) Rigid mold for bricks of cement treatment, (b) demolding a cement-treated brick

2.2.3 Samples Preparation of Cement-treated Samples with Bio-surface Treatments

MICP was used to treat the cement-treated samples to enhance their ability of resisting accelerated erosion. All samples were cleaned using a brush to remove loose sand particles and dust before the MICP treatment. The MICP process was also conducted in a batch tank reactor. The reactor included a plastic box containing samples, cementation media, sample supported shelf, and air

pumps to provide oxygen for bacteria. In the MICP process, the cement-treated samples were soaked into fresh bacteria solution with OD_{600} of 0.6 and then submerged in the cementation media of 0.5 M for 7 days' reaction.

The multiple MICP treatment method was following the same procedure used by the single MICP treatment. All treatments were carried out at ambient temperature of the laboratory. All samples were submerged into fresh water to remove residual, loose particles, and unbonded precipitates. Finally, the samples were oven dried until their weight reached constant. The dried samples were used for the following testing or treatments.

2.3 Erosion Methods

2.3.1 Long-term Erodibility of MICP-treated Soil

The long-term durability of MICP-treated soil on the erodibility was studied by exposing the soil boxes to the outdoor environment, which can simulate the long-term performance of MICP-treated soil on the erodibility. In addition, the samples for unconfined compression tests were also exposed to outdoor environment to study the changes of samples' strength over long-term. The exposed time of soil boxes and unconfined compression tests samples was 0 days, 12 days, 24 days, 48 days, and 96 days.

2.3.2 Rainfall Induced Erosion

Rainfall simulators are basic equipment to duplicate the physical characteristics of natural rainfall as closely as possible. It can be separated into two main types based on the way in which the raindrops are produced: 1) non-pressurized nozzle simulators; 2) pressurized nozzle simulators. In the non-pressurized nozzle simulators, water drops fall under the effect of gravity. These simulators are unrealistic for field use that a huge height (10 m) is needed for water drops to achieve the terminal velocity. The water drops strike the ground at a velocity much lower than the terminal velocity and with a lower kinetic energy, only if the simulator is hoisted very high. That is why the pressurized nozzle simulators are extensively preferred for studies at large area field.

In these simulators, raindrops were produced through single or multiple nozzles, while the drop intensities and velocities are usually exaggerated as the water is released under pressure. Since, a pressurized nozzle rainfall simulator was designed in this study.

(1) Design of rainfall simulator and erosion flume

Experimental design to perform erosion experiments consists of a rainfall simulator and an erosion flume (Figure 2-9). Rainfall simulator is made of a PVC frame attached with rain drop plate. The rain drop plate with multiple nozzles is installed on the PVC frame at a height of 1.0 m from the flume bed to ensure the terminal velocity of rain drops. Water is supplied from the water supply system. Laying under the rainfall simulator at a height of 5 cm from the ground is the erosion flume, which was fixed as slope of 10%.

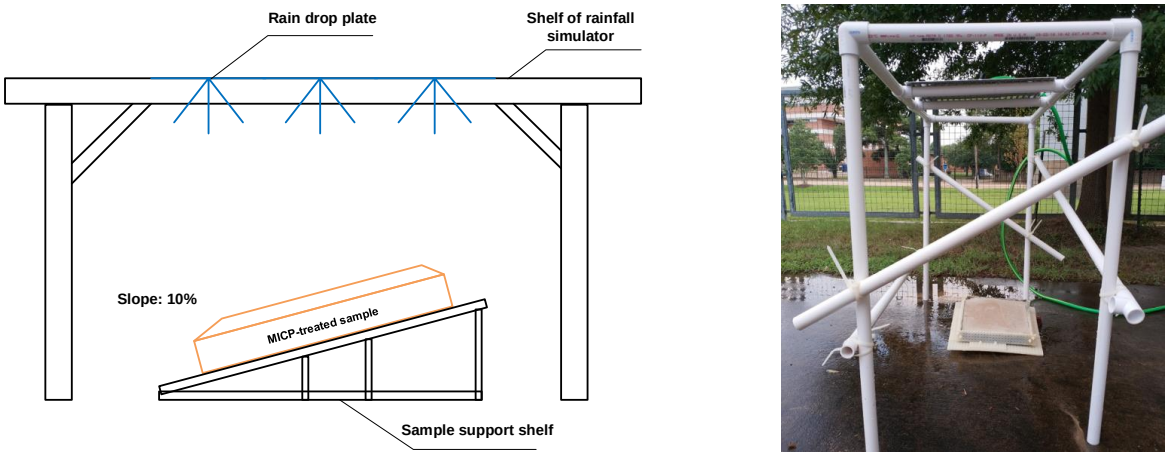

Figure 2-9. Sketch and photo of rainfall simulator and erosion flume

(2) Rainfall uniformity

The coefficient of uniformity (CuC) defined by (Christiansen 1941) is the most widely used measure of spatial uniformity, which is in percent as

$$\mathrm{CuC} = \left(1 - \frac{\sum_1^N |X_i - \bar{X}|}{N\bar{X}}\right) 100 \quad (4)$$

where X_i is rainfall amount at location i, $\bar{X}$ is average amount of rainfall and N number of points where measurement cups are placed over the flume to collect rainfall. The CuC is a useful index of spatial uniformity of rainfall. The more uniform the pattern of rainfall is, the closer CuC approaches to 100%. A rainfall can be considered uniform when CuC is higher than 80% (Moazed et al. 2010). However, the value of 70% has been accepted in some studies for large plot areas (Luk et al. 1993).

Table 2-1 shows the uniformity results. CuC were found higher than 80% for the four rainfall intensities. But CuC does not give any indication on the spatial pattern, which means that is possible for different patterns to get the same CuC value. So, the spatial patterns of rainfall were examined and the spatial relative rainfall intensity distribution maps were shown in Figure 2-10. It can be seen that the spatial distribution of rainfall can be considered uniform enough over the flume.

Table 2-1 Rainfall uniformity test

Rainfall intensity (mm/h)	CuC (%)
105	93.1
85	95.6
65	86.1
45	81.0

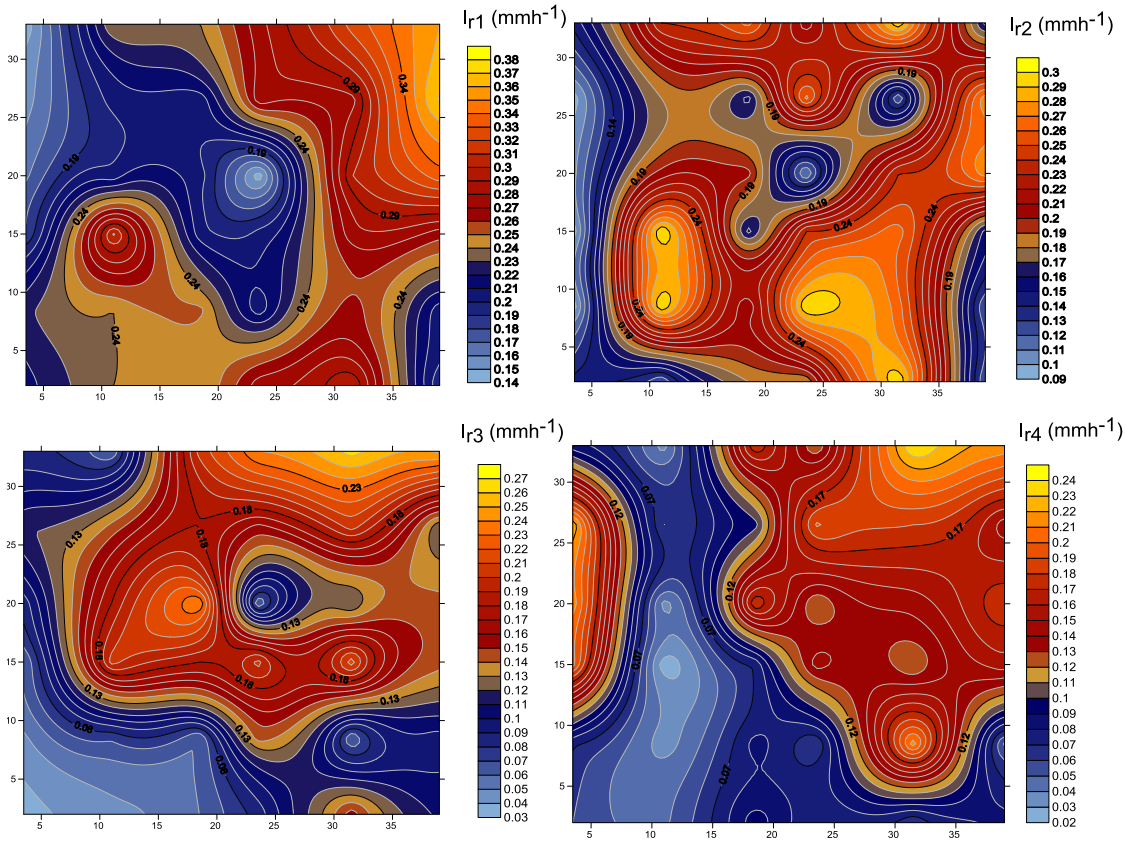

Figure 2-10. Spatial rainfall intensity distribution in the rainfall simulator with the for different rainfall intensity (I_r= Relative rainfall intensity)

(3) Raindrop size

The raindrop size was determined by flour pellet method (Bentley 1904) supported with an image processing technique. A 12.5-cm diameter circular pan filled with wheat flour (Figure 2-11(a)) was exposed to rainfall for each rainfall intensity (Figure 2-11(b)). Exposure time was restricted to 2 s to minimize coalescence of the pellets in the flour. Flour was dried for 12 h at105 ℃, then the pellets were sieved and photographed (Figure 2-11(c)). The photograph was then processed by an image processing software (Image-Pro Plus 6.0) to automatically distinguish and classify the raindrops based on the size of their surface area. Each raindrop was characterized by a circle area with a diameter to get the median diameter of raindrops.

(a) (b) (c)

Figure 2-11. Determination of raindrop size; (a) Flour cup, (b) Flour cup exposed to rainfall, (c) Flour pellets after oven drying

Raindrop size determined as detailed above was compared to those found in literature. An empirical equation fitted to data available in literature was given by (Van Dijk et al. 2002) as

$$D_{50} = \alpha R^{\beta} \tag{5}$$

Where R is rainfall intensity given in mm h^{-1}. Parameter in Eq. 5 have ranges of $0.8 \leq \alpha \leq 1.28$ and $0.123 \leq \beta \leq 0.292$ with which envelope curves in Figure 2-12 were graphed. The determined median raindrop sizes of this study were found within this range, which shows the performance of the rainfall simulator in terms of drop size.

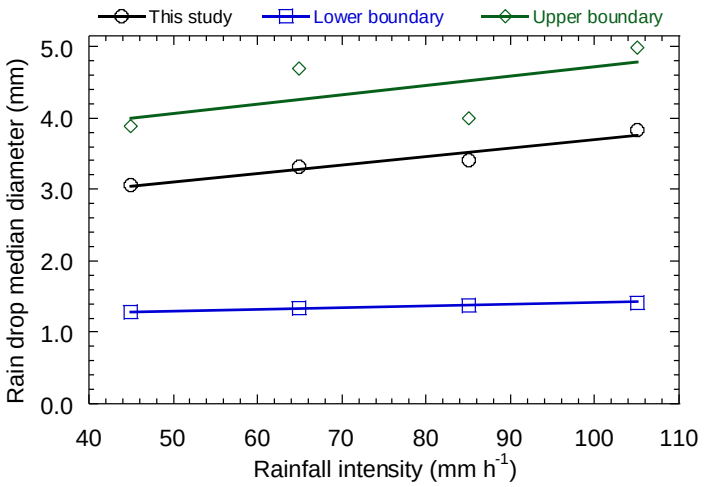

Figure 2-12. Changes in median diameter with rainfall intensity

2.3.3 Accelerated Erosion

The accelerated erosion was carried out on the bricks based on the testing method outlined by Walker. The erosion set up of this study is shown in Figure 2-13(a). A jet of water was sprayed onto the surface of brick at a constant pressure of 200 kPa and a constant distance of 470 mm. The erosion depth was recorded as Figure 2-13(b) showed at frequent intervals through a 60 min period. And then the maximum erosion rate of the sample was determined by the following Eq. (6):

$$\text{Erosion rate} = \frac{maximum\ erosion\ depth}{height\ of\ brick} \times 100\% \tag{6}$$

(a)

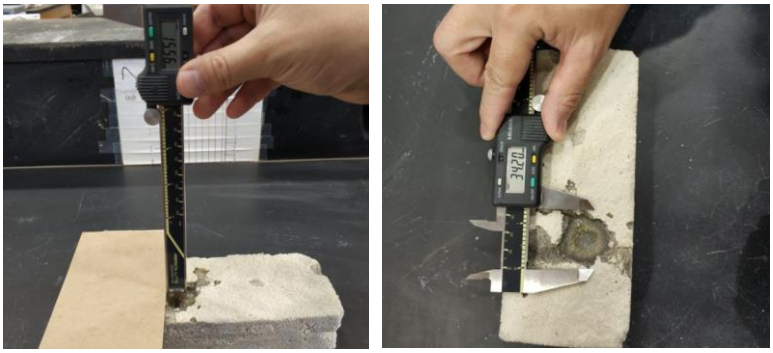

(b)

Figure 2-13. Accelerated erosion test; (a) Accelerated erosion set up, (b) measuring the eroded area of bricks.

2.4 Testing Methods

2.4.1 The Pocket Erodometer Testing

The pocket erodometer testing (PET) is a simple and which can be performed in a relatively short time using a cheap, compact, and light device. This testing provides a quick field estimate of the erodibility of the soil sample. The pocket erodometer directs a horizontal jet of water repeatedly at the vertical face of the sample. The depth of the hole in the surface of sample produced by 20 jet applications is recorded and compare with an erosion function apparatus (EFA) erosion chart to determine the erodibility category of the soil. This category allows the engineers to get preliminary decisions in erosion related work. A water gun as shown in Figure 2-14 was selected as jet generating device because of its small size, its light weight, and its simplicity.

Figure 2-14. Photo of water gun used in PET testing

Standard pocket erodometer test procedure (Briaud et al. 2011) as follows was applied in this study. The calibration of the nozzle exit velocity was obtained before beginning each testing session. The nozzle velocity was ensured as 8 $\pm$0.5 m/s for each test.

1) Place the sample horizontally on a flat surface. Note: The test cannot be run with the jet pointed vertically.

2) Smooth the surface to remove any uneven soil. You want to begin with a smooth and vertical surface, so that it is easy to measure the erosion depth.

3) Hold the pocket erodometer (PE) pointed at the smooth end of the sample, 50 mm away from the face.

4) Keeping the jet of water from the PE aimed horizontally at a constant location, squeeze the trigger 20 times at a rate of 1 squeeze per second, forming an indentation in the surface of the sample. Each squeeze should fully compress the trigger and then the trigger should be fully released before it is recompressed.

5) Using the end of a digital caliper or an appropriate measuring tool, measure the depth of the hole created.

6) The test should be repeated at least 3 times in different locations across the face of the sample and an average should be used to ensure a good estimate.

7) Determine the erosion category using Figure 12-15 (Briaud et al. 2011).

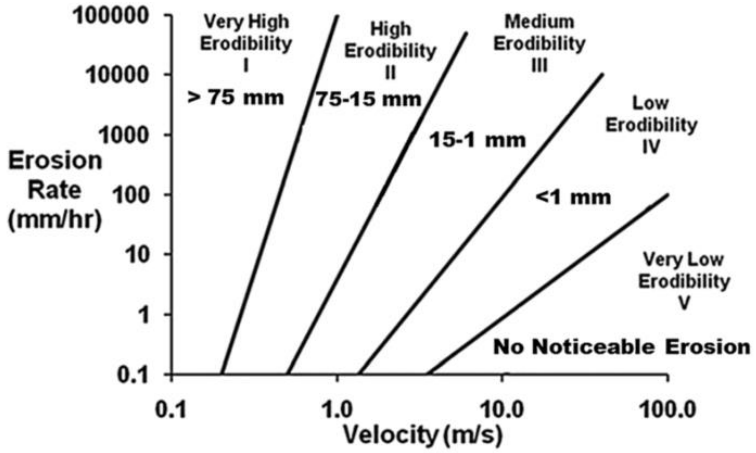

Figure 2-15. PET erosion depth ranges shown on EFA categories (Briaud et al. 2011).

2.4.2 Soil Stiffness Gauge (SSG) Testing

The non-destructive SSG tests were conducted to test the stiffness of soil samples in accordance with ASTM D6758 using a Humboldt GeoGauge (shown in Figure 2-16). Two measurements will

be made at each location within a 0.1-m radius. Testing with the SSG will be conducted directly on the MICP-treated geomaterials.

Figure 2-16. Photograph of Humboldt GeoGauge.

2.4.3 Dynamic Cone Penetrometer (DCP) Testing

The DCP tests will be conducted using the DCP instrument (shown in Figure 2-17) at each location in accordance with ASTM D 6951. The dynamic penetration index (DPI) obtained from the DCP will be computed as the mean penetration (mm per blow) over a depth of 150 mm. Testing with the DCP will be conducted directly on the MICP-treated geomaterials.

Figure 2-17. Photograph of dynamic cone penetrometer

2.4.4 Roughness Testing

The LS-40 Portable 3D Surface Analyzer as shown in Figure 2-18(a) is a 3D surface measurement and analysis device, which scans a 4.25" by 6" or 10" areas and produces a high resolution (0.01mm) digital surface structure with an intensity image and a surface depth (height) related range image. LS-40 provides the data to calculate mean profile depth (MPD) and 3D views by processing profiles over the entire scanned surface according to ASTM E1845 specifications.

As shown in Figure 2-18(b), the measured profile is divided for analysis purpose into segments each having a base length of 100 mm. The segment is future divided in half and the height peak in each half segment is determined. The difference between that height and the average level of the segment is calculated. The average value of these differences for all segments making up the measured profile is reported as the MPD. The MPD values were used to describe the roughness of samples' surface in this study.

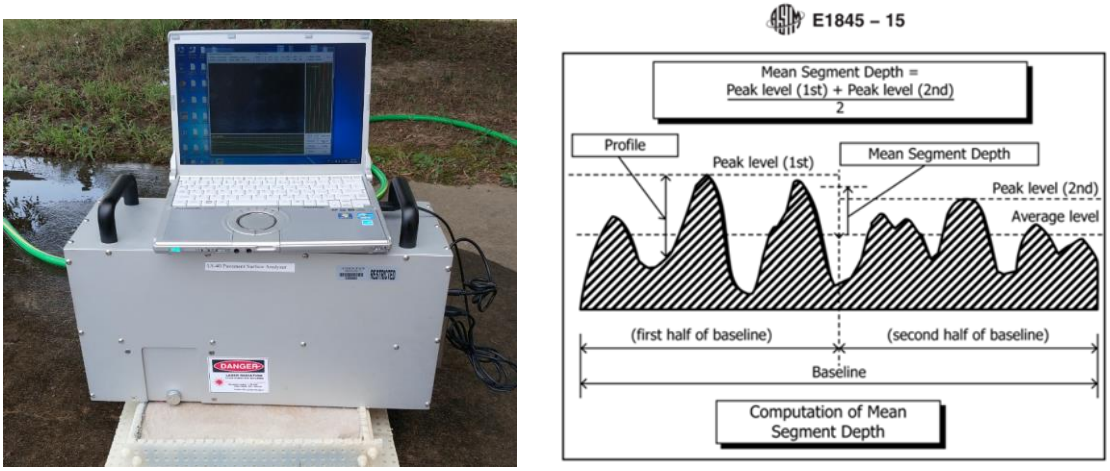

Figure 2-18. Surface Analysis; (a) Photograph of LS-40 Portable 3D Surface Analyzer, (b) Computation procedure of mean segment depth.

2.4.5 Unconfined compression tests

The samples for unconfined compression tests were cylinder-shaped with 2H:1D ratio. The unconfined compression tests were conducted under strain controlled conditions at a uniform loading rate of 1.5%/ min in accordance with ASTM D2166.

2.4.6 Brick Compressive Strength Testing

The brick compression tests were conducted on cemented-treated bricks, and cement-treated bricks with biosurface treatment. Each test sample was cut into halves along the width direction. As shown in Figure 2-19, these two halves were stacked along the surface perpendicular to the cutting surface. The testing procedure applied on the stacked halves was followed the testing method of ASTM C67-02c and the vertical load was conducted under strain control conditions at a uniform loading rate of 1.5%/min.

Figure 2-19. Brick compressive testing system for stacked two halves

2.4.7 Four Point Bending Testing

The four-point bending tests as shown in Figure 2-20 were conducted to study the flexure behavior of bricks. The samples were located on two adjusted supports that were 152.4 mm apart from each other, and the vertical load was applied on top two supports at middle of the specimen with 50.8 mm distance. Following testing method of ASTM D6272, the vertical load was conducted under strain control conditions at a uniform loading rate of 1.5%/min until beam fails.

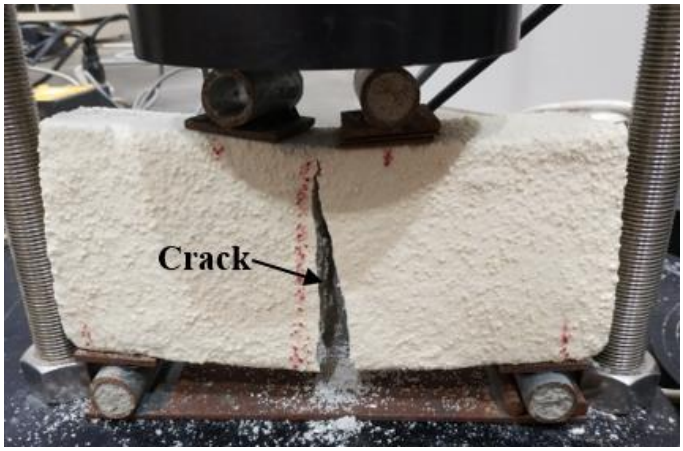

Figure 2-20. Four point bending testing system

2.4.8 Resistance to Water Absorption

Resistance to water absorption was determined as the average of three treated samples. The dry mass (m_d) of the bricks was recorded at first. Then the bricks were totally submerged in water at ambient temperature for 24 h. Took out the bricks and weighted immediately as the saturated mass (m_s). The water absorption (W_a) of the bricks was calculated by:

$$W_a = \frac{m_s - m_d}{m_d} \times 100\% \quad (7)$$

2.4.9 $CaCO_3$ Content Tests

The $CaCO_3$ precipitated in the MICP-treated sample was determined by acid-washing method. In the acid-washing method, the samples were crushed and collected at the different locations of the specimens. All the collected samples were oven dried and washed with an HCl solution (0.1 M) to dissolve precipitated carbonates, rinsing, draining, and oven drying. The difference in weight between the dry MICP-treated samples and the dry samples after acid washing was the weight of the carbonates that were precipitated in the sample.

2.4.10 SEM Analysis

Formation of $CaCO_3$ precipitation in the MICP-treated bio-specimen was examined by scanning electron microscopy (SEM) (Lyra 3, TSECAN Inc.). The tested samples were oven-dried overnight at 105 ℃before testing and mounted on the stubs with adhesive carbon conductive tabs. Then, the prepared SEM samples were imaged by secondary electron detection.

3. Results/ Findings

3.1 Long-term Erodibility of MICP-treated Soil

Mississippi local sand and Ottawa silica sand were used to perform long-term erodibility of MICP-treated sand. The soil boxes were made by Mississippi local sand and UCS tests samples were made by Ottawa silica sand.

The erodibility of MICP-treated soil boxes was tested by in-site pocket erodometer after exposing to outdoor environment. The results showed that the erosion depth reached on the surface of soil boxes were close to 0 mm not only before exposing but also after 12, 24, 48, and 96 exposed days. The erosion categories were determined using Figure 2-15. No noticeable erosion appeared on the surface of MICP-treated soil subjected to 20 jet impulses generating 8 m/s nozzle velocity at one second intervals, which means MICP-treated soil had very low erodibility over long-term under PET method.

Figure 3-1 showed a box plot of unconfined compression strength (UCS) of MICP-treated samples as a function of exposed time to outdoor environment. Each box showed the median value and ± 25% of the UCS population as the top and bottom of the box. The lines extending from the top and bottom of each box mark the minimum and maximum UCS. The outlier was shown as an individual point. From the box plot, the UCS of MICP-treated samples decreased gradually with longer exposed time to outdoor environment. Moreover, the MICP-treated samples showed a rapid decrease at early stage. The average UCS of MICP-treated was 1200 kPa before exposing to outdoor environment. But after 12 exposed days, the MICP-treated samples only achieved 700 kPa

of UCS, 41.7% decrease of UCS was caused by exposing to outdoor environment. The results indicated that the MICP-treated samples were weak to resist long-term outdoor erosion.

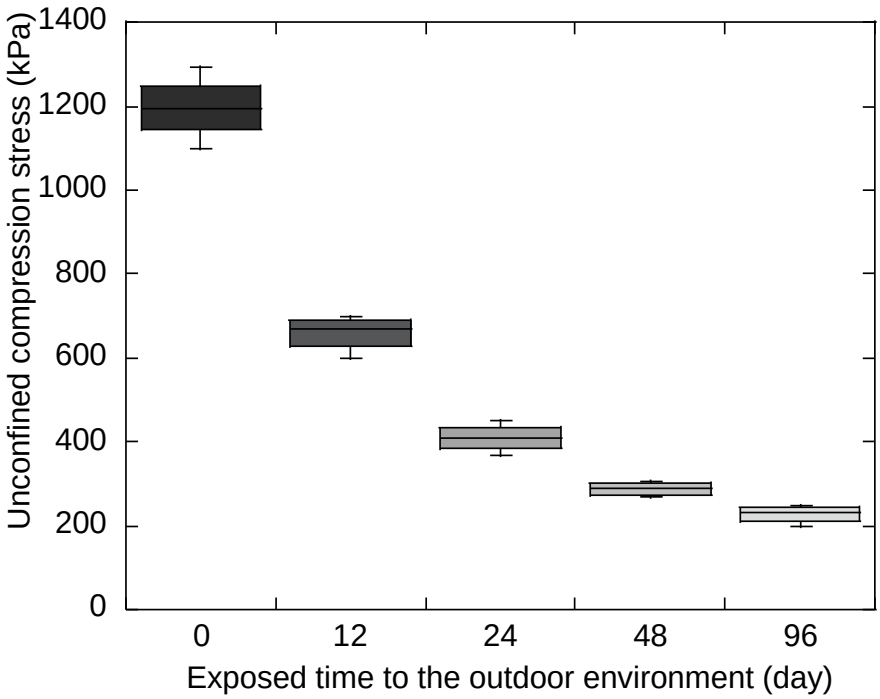

Figure 3-1. Unconfined compression strength of MICP-treated soil with different exposed time to outdoor environment

3.2 SSG and DCP Measurements on MICP-treated Soil

In order to obtain the stiffness and mean penetration over a depth of 150 mm of MICP-treated soil, SSG and DCP measurements were conducted on the MICP-treated soil boxes. However, the soil boxes were smashed into pieces by self-weight of SSG and DCP as shown in Figure 2-17 in the experimental process. This phenomenon should be caused by the brittle behavior of MICP-treated soil (Zhao et al. 2014b). Since, SSG and DCP methods were not suitable to test MICP-treated soil. The MICP-treated soil boxes disintegrated during testing and no value was obtained from these two testing methods.

3.3 Rainfall Induced Erosion of MICP-treated soil

Mississippi local sand was used in this study to perform the rainfall induced erodibility of MICP-treated soil. Before the formal experiments, rainfall with four different intensity was examined by eroding the MICP-treated soil that was treated by 0.25 M Ca cementation media concentration for 24 h. No noticeable erodibility could be observed on the MICP-treated soil under the rainfall with intensity of 45 mm/h, 65 mm/h, and 85 mm/h. As shown in Figure 3-2, the MICP-treated soil was eroded seriously by the rainfall with intensity of 105 mm/h. Since, in order to obtain noticeable erodibility, the rainfall with intensity of 105 mm/h was selected to perform the rainfall induced erosion of MICP-treated soil in this study.

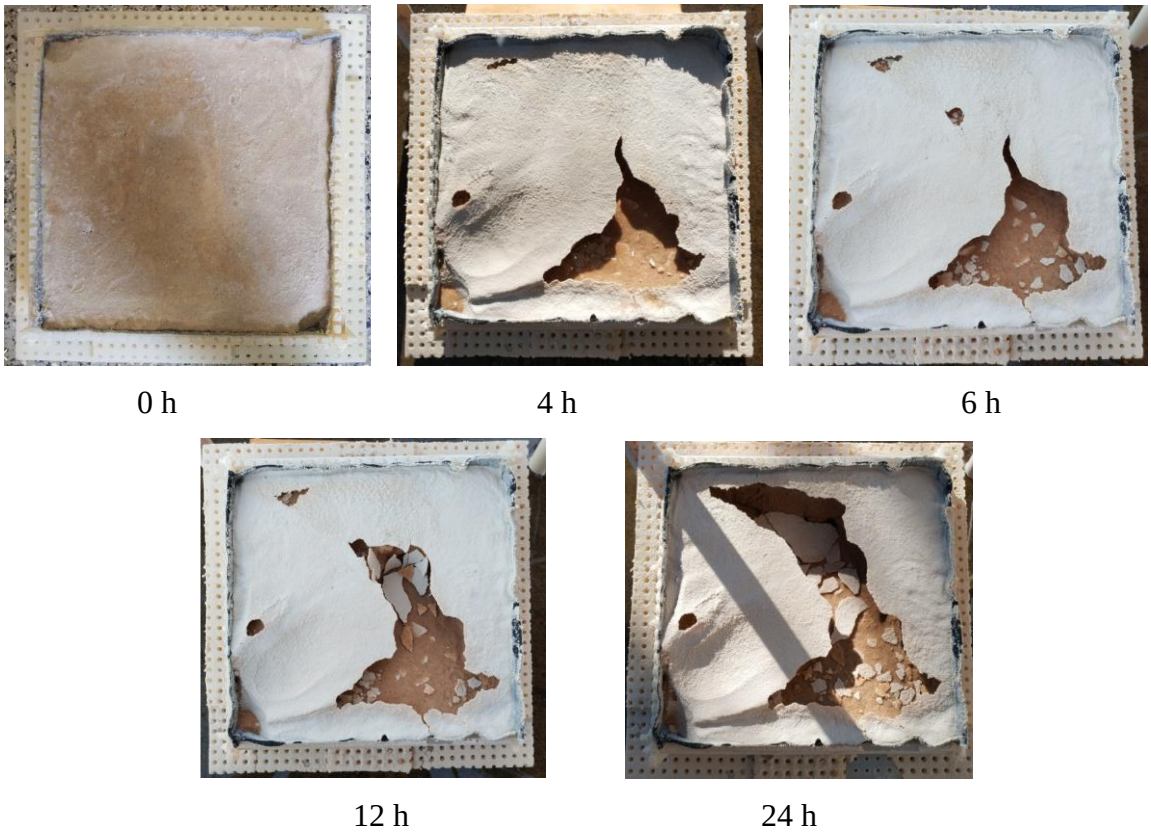

Figure 3-2. Photograph of MICP-treated soil (0.25 M Ca) after 105 mm/h rainfall induced erosion under different eroded time

In order to obtain the properties of MICP-treated soil under rainfall induced erosion, the properties of MICP-treated samples were compared with soil samples made through cement modification.

The proportion of cement in this part was 5% by weight of dry sand, and the concentration of cementation media for the MICP-treated samples was 0.5 M Ca.

No visible erodibility could be observed on the surface of MICP-treated and cement-treated samples after 24-h rainfall induced erosion. Since, roughness testing was conducted on samples to investigate the subtle erodibility caused by rainfall induced erosion. Soil surface roughness is an important parameter in understanding the mechanisms of soil erosion by water. Three dimensional (3D) measurements were applied by laser-scanner device in this study. Roughness of samples was tested after eroded time of 0 h, 1 h, 2 h, 4 h, 6 h, 12 h, and 24 h, respectively. To investigate the roughness of soil surface, 3D views and mean profile depth were analyzed.

For MICP-treated samples, Figure 3-3 showed the 3D surface views before and after 24-h rainfall induced erosion. The eroded surface looked smoother than the uneroded surface, maybe because the powdery bonds, unbonded minerals or loose bonded calcite were washed away by water.

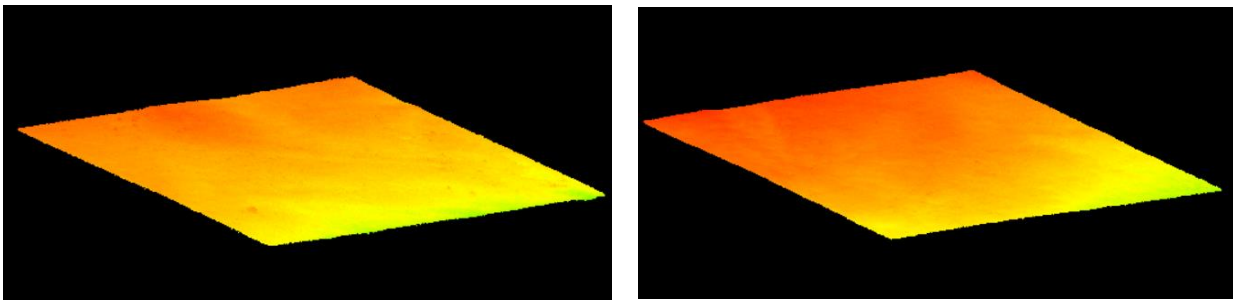

(a) (b)

Figure 3-3. 3D surface views of MICP-treated sample; (a) before rainfall induced erosion, (b) after 24-h rainfall induced erosion.

Similar results could be obtained from Figure 3-4, which showed the MPD values of MICP-treated sample as a function of rainfall induced eroded time. Higher MPD value represented a textured surface, which means a more rough surface. The MPD values on surface of MICP-treated sample decreased gradually along with longer rainfall induced eroded time. 16.7% decrease of MPD value happened after 24-h rainfall induced erosion. A more smooth surface of MICP-treated sample was

caused by rainfall. When the soil sample was treated by MICP, a part of $CaCO_3$ precipitation was only attached to the surface of sand particles that may not bond the sand particles, thus easily be eroded by rainfall and resulted in smooth surface.

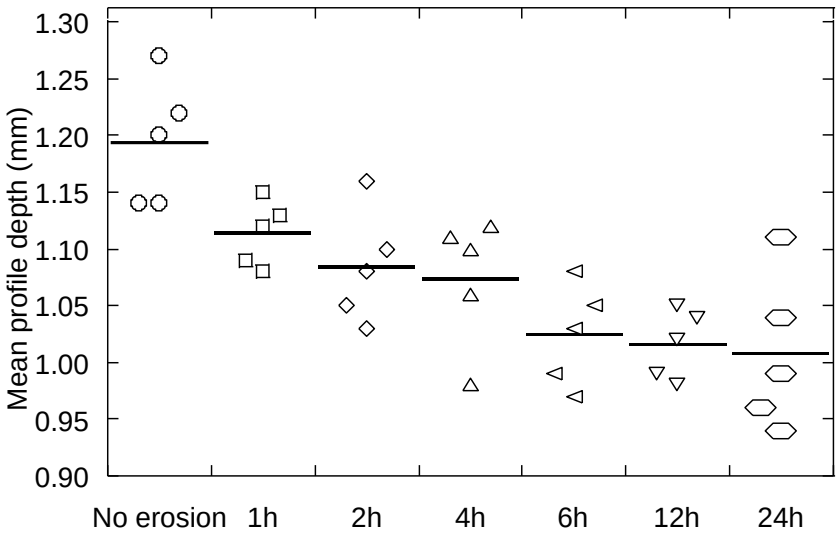

Figure 3-4. Mean profile depth on the surface of MICP-treated sample as a function of rainfall induced eroded time

For cement-treated samples, the opposite results were induced by rainfall. From Figure 3-5, the 3D views of cement-treated sample became more rough after 24-h rainfall induced erosion.

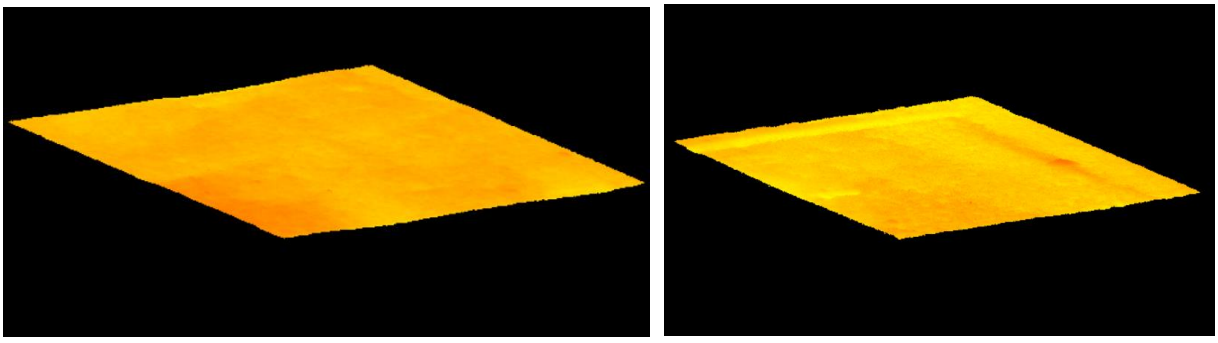

(a) (b)

Figure 3-5. 3D surface views of cement-treated sample (a) before rainfall induced erosion; (b) after 24-h rainfall induced erosion

The same conclusion could be summarized from Figure 3-6. The MPD values on surface of cement-treated samples kept increasing as the rainfall induced eroded time growing. 75% increase of MPD value happened because of 24-h rainfall induced erosion. A rough surface was induced by rainfall. This phenomenon could be caused by the hydraulic strength of cement during the rainfall induced erosion process. The early strength of cement in this study gain allowed the various curing times ranged from 7 to 21 days. The cement-treated samples were cured for 7 days in a constant humidity of 100% before the rainfall induced erosion test. Loose bonded sand particles were washed away by rainfall at the early stage of the erosion, meanwhile, the strength of cement-treated sample kept increasing during the erosion process to resist the erosion. Afterwards, a rough surface was formed at the later stage of rainfall induced erosion.

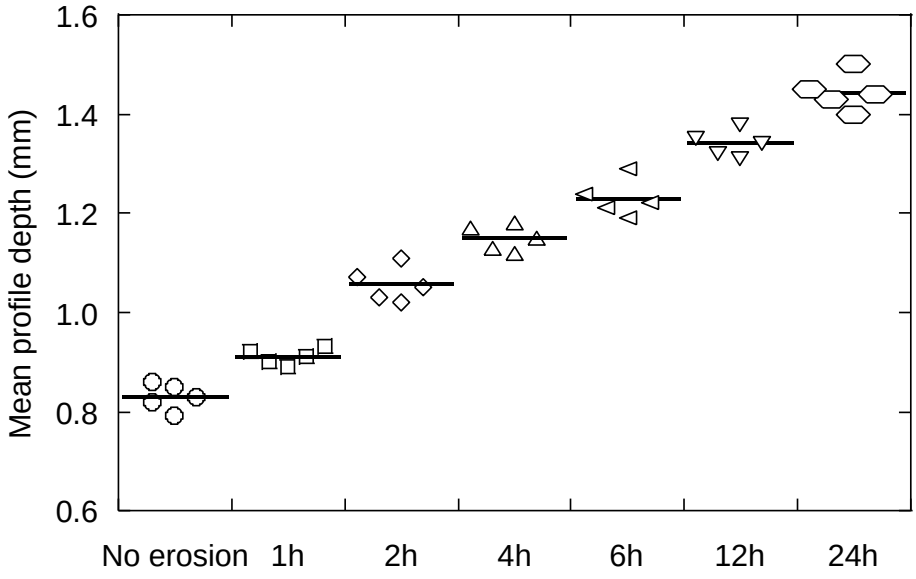

Figure 3-6. Mean profile depth on the surface of cement-treated sample as a function of rainfall induced eroded time.

3.4 Accelerated Erodibility of MICP-treated Soil

3.4.1 Cement-treated Soil with Bio-surface Treatments

Ottawa silica sand was used in this part. The proportion of cement was 5% and 10% by weight of dry sand, and the concentration of cementation media for the bio-surface treatments was 0.5 M Ca.

(1) Flexure behavior

The flexure stress and strain relationship for cement-treated samples with bio-surface treatments was shown in Figure 3-7. The flexure strength increased from 500 kPa to 750 kPa when single bio-surface MICP treatment was applied on the cement-treated samples. Moreover, the flexure strength kept increasing along with more bio-surface treatments. The cement-treated samples achieved 1200 kPa flexure strength with triple bio-surface treatments, which was nearly 140% increase compared with cement-treated samples without bio-surface treatments. The results indicated that the bio-surface treatments enhance the flexure strength of cement-treated samples significantly.

The failure cracks pattern of all cement-treated samples was studied as shown in Figure 2-20. Cracks were not shown when the load was increased initially. The cracks initially extended from the bottom to the top of the samples in the bending tests. When the cracks fully extended to the top edge of the samples, the cement-treated samples failed. All samples failed into halves and the fracture crack was parallel to loading direction, which illustrated that the cement-treated samples failed in bending mode. The failure patterns of those beam samples were similar to plain concrete beam reported by Yun (2013).

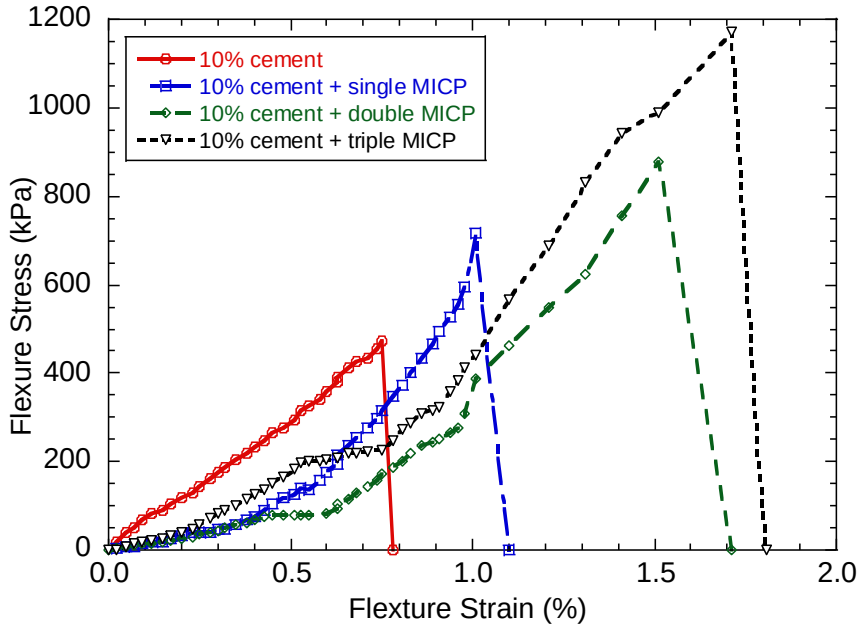

Figure 3-7. Flexure stress-strain curves for cement-treated sample and cement-treated samples with bio-surface treatments

(2) Brick compression strength

The stress and strain relationship for cement-treated sample and cement-treated samples with bio-surface treatment obtained from brick compression strength testing was shown in Figure 3-8. Enhancement of brick compression strength was induced by the proposed bio-surface treatments. Significant increase in the compression strength was achieved for the cement-treated samples with triple bio-surface treatments, which was nearly 100% increase. That was anticipated since the precipitated $CaCO_3$ produced by the bio-surface treatments strengthened the cement-treated samples. More precipitate could be produced by multiple bio-surface treatments, since more enhancement on the compression strength of samples could be achieved by the multiple-treatment method.

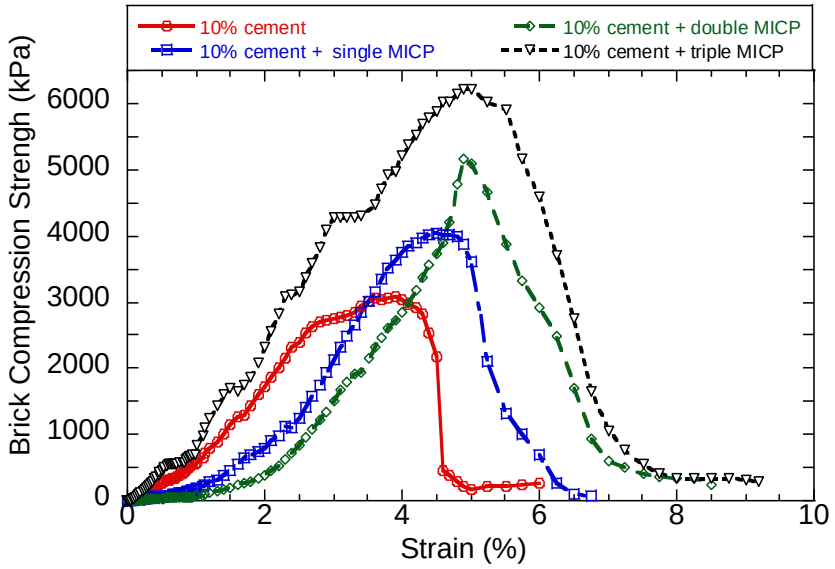

Figure 3-8. Stress-strain curves for cement-treated sample and cement-treated samples with bio-surface treatment

(3) Erosion resistance

Accelerated erosion testing was undertaken on cement-treated samples and cement-treated samples with bio-surface treatment. Cement-treated sample with triple bio-surface treatments did not experience any measurable erosion over a 60 min time period. The appearance of cement-treated samples with bio-surface treatments at the end of erosion testing was shown in Figure 3-9.

Figure 3-9. Surfaces of single, double, and triple bio-surface treated cement-treated samples after accelerated erosion

The maximum erosion rate was shown in Figure 3-10. In comparison, the 5% cement-treated sample demonstrated rapid erosion and almost none withstood the test of 60 min period. The maximum erosion rate decreased when cement proportion was increased. When bio-surface treatments were applied on the 10% cement-treated samples, the maximum erosion rate decreased along with more treatments. No erosion could be measured after the cement-treated sample was triple treated by bio-surface treatments.

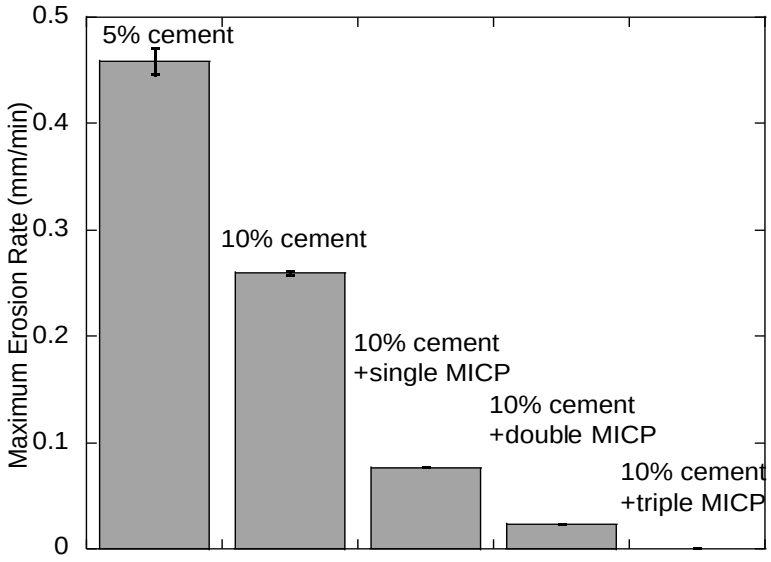

Figure 3-10. Maximum erosion rate for cement-treated samples and cement-treated samples with bio-surface treatments

(4) Water absorption

Water absorption testing was undertaken on the cement-treated samples and cement-treated samples with bio-surface treatments, the results of which was shown in Figure 3-11. Compared with 5% cement-treated samples, 10% cement improved the resistance to water absorption. When bio-surface treatments were applied on the 10% cement-treated samples, the precipitated $CaCO_3$ provided a higher resistance to water absorption than untreated cement-treated samples. These surface-treated samples were therefore likely to be more durable. The cement-treated sample with triple bio-surface treatments achieved a 5% lower water absorption than untreated 10% cement samples.

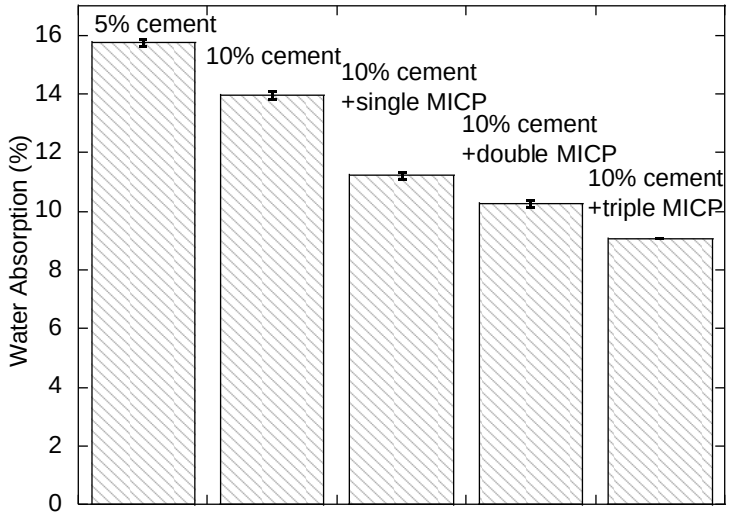

Figure 3-11. Water absorption for cement-treated samples and cement-treated samples with bio-surface treatment.

3.4.2 MICP-treated soil

Ottawa silica sand was used in this part. The concentration of cementation media for the bio-surface treatments was 0.5 M Ca in this part.

(1) $CaCO_3$ content

As shown in Figure 3-12, multiple MICP treatments significantly improve the $CaCO_3$ content, especially in the first three treatments. These improvements enhanced the strength of MICP-treated samples. Triple MICP treatments at most were performed to improve the MICP-treated soil in this study.

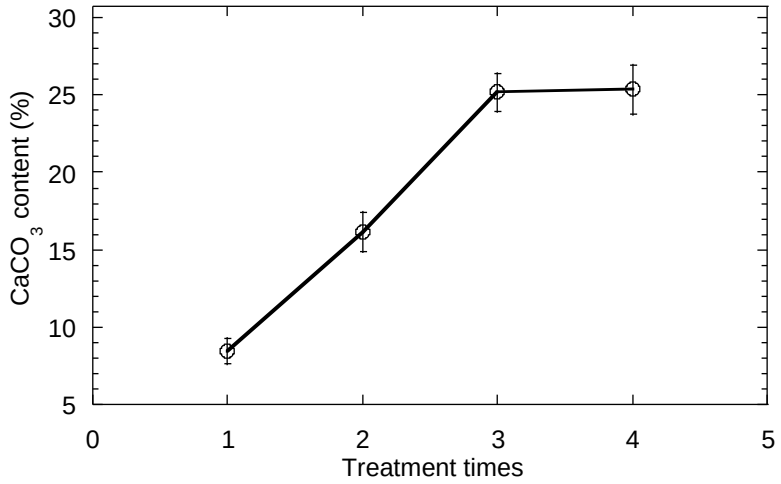

Figure 3-12. $CaCO_3$ content of MICP-treated sand as a function of treatment times

As shown in Figure 3-13(a), the individual $CaCO_3$ crystals of single MICP-treated samples had similar size and separately distributed. However, for quadruple MICP-treated samples as shown in Figure 3-13(b), the $CaCO_3$ shell coated the surface of the sand particles. The boundary between each MICP treatments was clearly observed. With more MICP treatments, $CaCO_3$ crystals filled in the gaps and acted as bridges among the sand particles that contribute to the strength of MICP-treated soil.

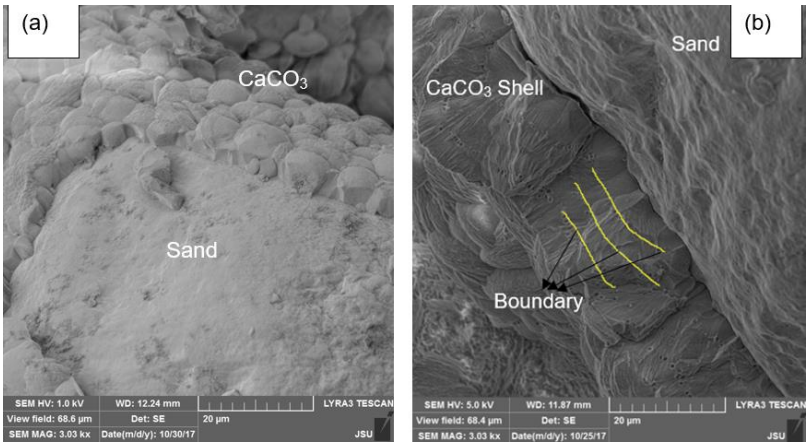

Figure 3-13. SEM images of MICP bonded sand particles; (a) Single MICP treated, (b) Quadruple MICP treated.

Figure 3-14(a) showed the SEM image of MICP-treated sample reinforced with 0.3% fiber. The fiber acted as bridge and tension members between soil particles and calcium carbonate, that improve the bonding between soil particles. When local cracks appeared on MICP-treated sample with fiber reinforcement, fibers across the cracks took the tension within the soil due to the fiber-soil friction, which effectively impeded further development of cracks, and thus improved the resistance of soil to the force applied. Moreover, fiber reinforcement induced more calcium carbonate (Figure 3-14(b)), because that the bacteria attach on fiber and thus form the mineral cores to attract more calcium carbonate crystals. The addition of fiber in the MICP process had the potential to increase the ductility of the MICP-treated soil (Li et al. 2015).

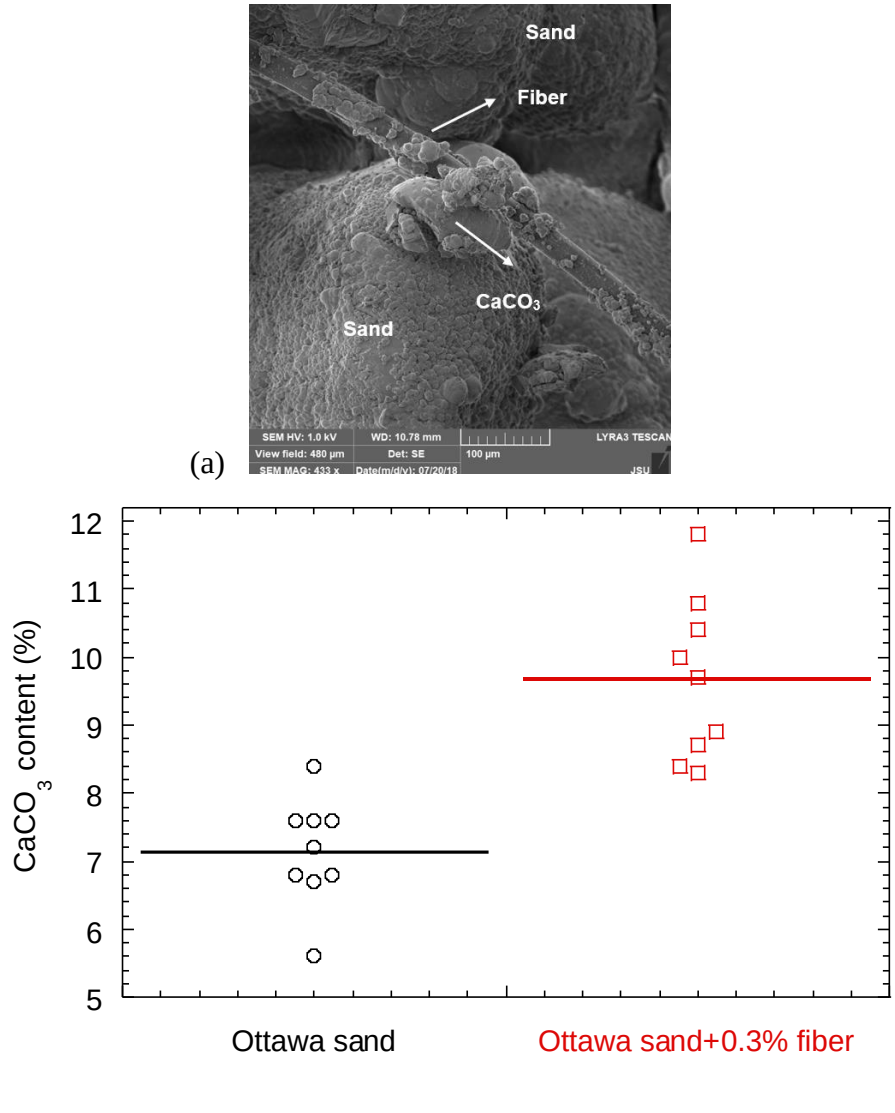

Figure 3-14. (a) SEM image of MICP-treated sand particles with fiber reinforcement; (b) $CaCO_3$ content of unreinforced and fiber reinforced MICP-treated samples.

(2) Flexure behavior

The stress-strain curves obtained from four-point bending tests for MICP-treated samples were shown in Figure 3-15. Compared unreinforced with 0.3% fiber reinforced single MICP-treated samples, flexure strength was not improved, whereas flexure strain was improved a lot by the addition of 0.3% fiber. The results indicated that addition of fiber could contribute to the improvement of ductility.

For the effect of multiple MICP treatments on flexure behavior of MICP-treated samples, the single MICP-treated sample had peak flexure strength around 1100 kPa, and the peak flexure strength increased to 1600 kPa and 2600 kPa after double and triple MICP treatments, respectively. Multiple MICP treatment can increase more $CaCO_3$ precipitation and those $CaCO_3$ can bond the sand particles stronger. Therefore, the strength of multiple MICP-treated soil increased with treatment cycles.

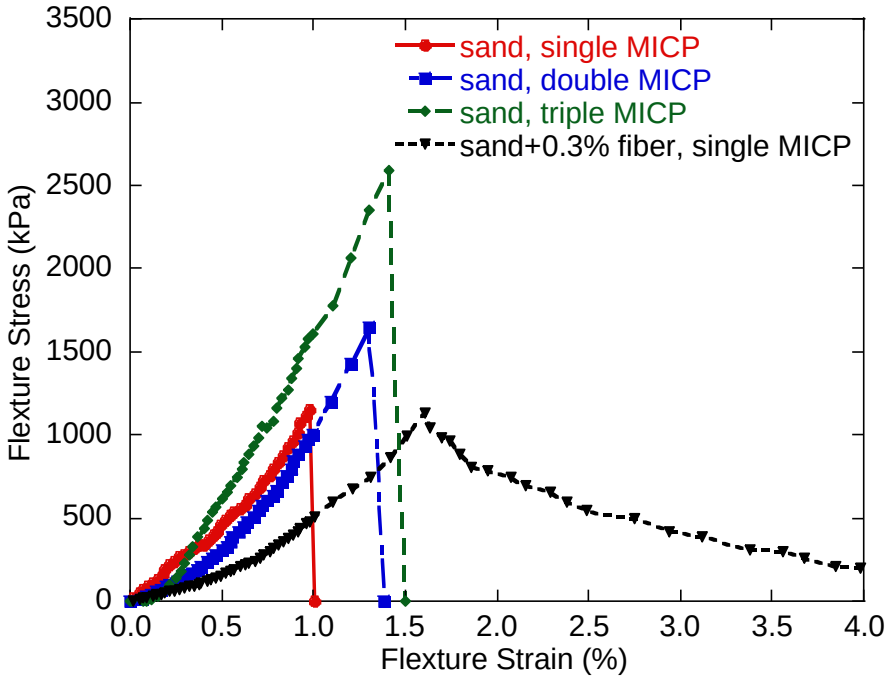

Figure 3-15. Flexure stress-strain curves for MICP-treated samples

(2) Brick compression strength

Figure 3-16 showed the stress-strain curves of brick compression strength for MICP-treated samples. Compared with unreinforced single MICP-treated samples, the brick compression strain of 0.3% fiber reinforced single MICP-treated samples was enhanced by the extra fiber. The peak compression strength of single MICP-treated sample was 2000 kPa, which was improved to 5000 kPa and 7000 kPa, almost 150% and 250% enhancement after double and triple MICP treatments. The results indicated that the addition of 0.3% fiber could improve the ductility of MICP-treated samples and multiple MICP treatments could help samples achieve higher strength.

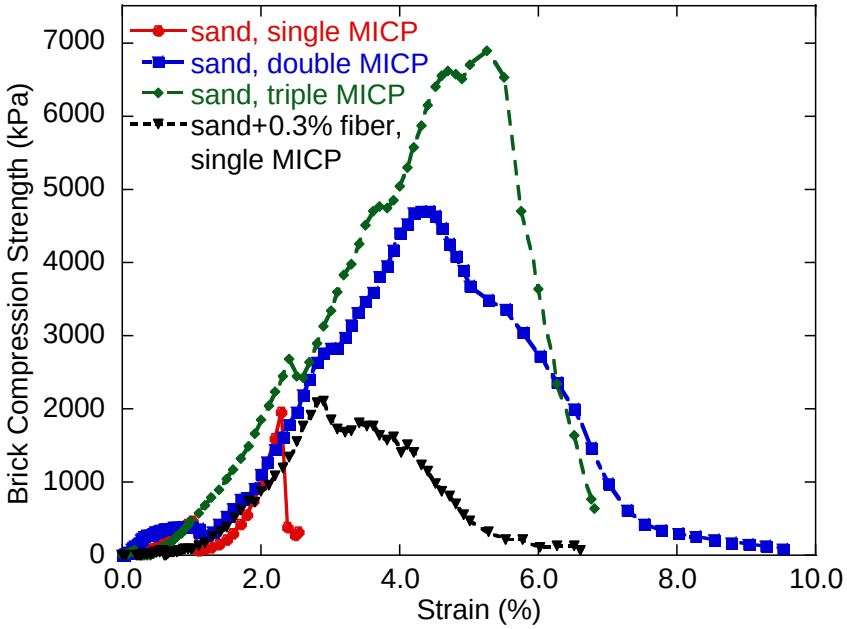

Figure 3-16. Stress-strain curves of MICP-treated samples.

(3) Erosion resistance

From the appearance of MICP-treated samples at the end of erosion testing as shown in Figure 3-17, the double and triple MICP-treated samples did not experience any measurable erosion over a 60 min time period. Figure 3-18 showed the maximum erosion rate of MICP-treated samples, the maximum erosion rate of single MICP-treated samples reduced from 0.16 mm/min to 0 mm/min after triple MICP treatment cycles applied on the samples. The 0.3% fiber addition also reduced the maximum erosion rate to 0.075 mm/min from 0.16 mm/min for single -treated samples. The

results indicated that multiple MICP treatments method and fiber addition made contributions to reduce the erosion of MICP-treated samples.

Figure 3-17. Surfaces of single, double, and triple MICP-treated samples after accelerated erosion.

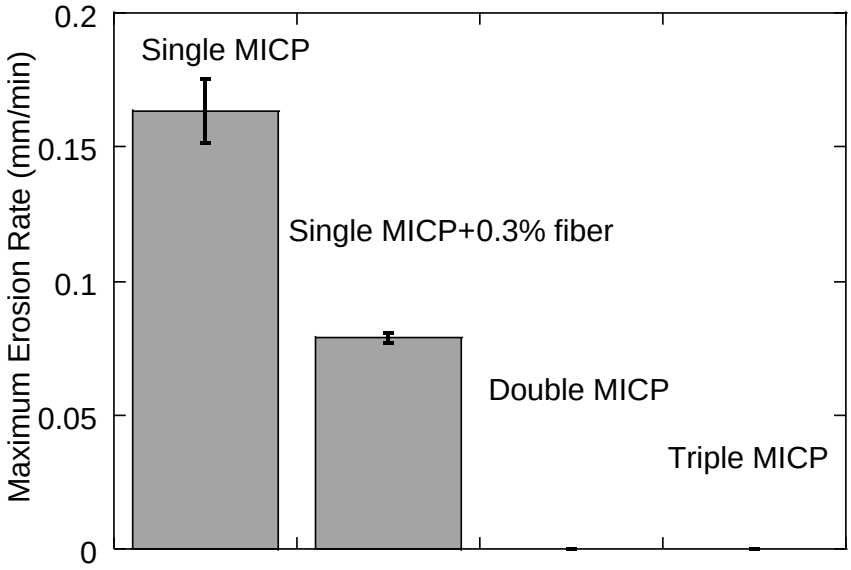

Figure 3-18. Maximum erosion rate for cement-treated samples

(4) Water absorption

The results of water absorption testing for MICP-treated samples were shown in Figure 3-19. The addition of 0.3% fiber had less help to reduce the water absorption of MICP-treated samples. But extra MICP treatments on soil samples improved the resistance to water absorption significantly. Denser precipitated $CaCO_3$ was produced by multiple MICP treatments, which provided a higher resistance to water absorption than single MICP-treated samples. The triple MICP-treated samples achieved a 6% lower water absorption than single-treated samples, which means the multiple MICP-treated samples were more durable.

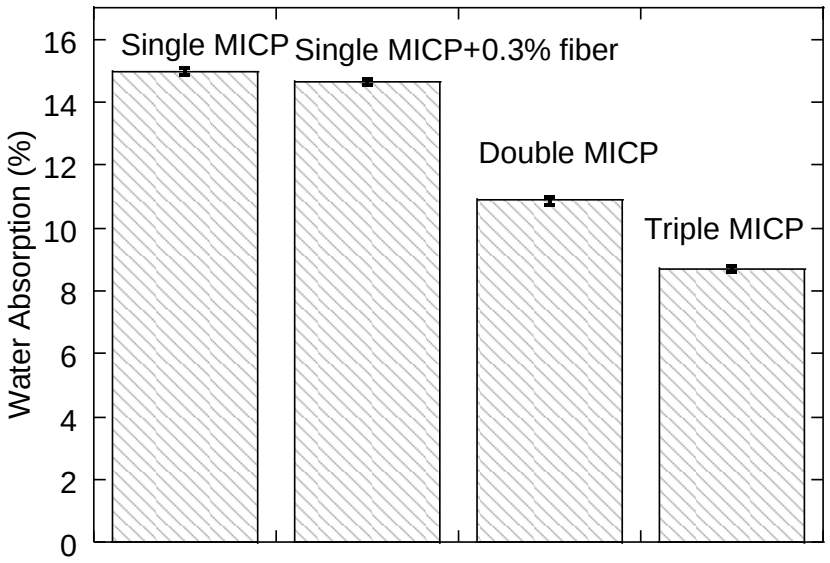

Figure 3-19. Water absorption for MICP-treated samples

4. Impacts/Benefits of Implementation (actual, not anticipated)

The results of this study bring an important conclusion that MICP-treated soil was weak to resist long-term erosion of exposing to outdoor environment. However, MICP-treated material was strong to resist rainfall induced erosion and accelerated erosion. Especially the bio-surface treatments could enhance the strength of cement-treated samples significantly, further improve the resistance to accelerated erosion and water absorption. In addition, fiber reinforcement of MICP-treated samples improved the resistance to accelerated erosion, whereas, multiple MICP treatments

method could contribute to the improvement of both resistance to accelerated erosion and water absorption.

5. Recommendations and Conclusions

This study intended to develop an alternative approach for armoring the riverbed with biocementation through MICP to mitigate soil erosion. Long-term erosion exposed to outdoor environment, rainfall induced erosion, and accelerated erosion were conducted on MICP-treated samples to prove the feasibility of the MICP technique for potential applications in prevention of bridge scour and road shoulder erosion. The experimental work and discussion about the testing results indicated that exposing to outdoor environment could result in sharp decrease on UCS for MICP-treated samples. But the MICP-treated samples had better resistance to rainfall induced erosion. The bio-surface treatment gave significant help for cement-treated samples to resist accelerated erosion and water absorption, especially the multiple bio-surface treatments method, no erosion could be measured and 5% lower water absorption was achieved after the cement-treated sample was triple treated by bio-surface treatments. The pure MICP-treated samples were also good at resisting accelerated erosion and water absorption. Furthermore, fiber addition and multiple MICP treatments could improve their resistance. The maximum erosion rate of single MICP-treated samples reduced from 0.16 mm/min to 0 mm/min after triple MICP treatment cycles applied on the samples. The 0.3% fiber addition also reduced the maximum erosion rate to 0.075 mm/min from 0.16 mm/min for single -treated samples. For resistance to water absorption, the addition of 0.3% fiber had less help to reduce the water absorption of MICP-treated samples. But extra MICP treatments on soil samples improved the resistance to water absorption significantly. The triple MICP-treated samples achieved a 6% lower absorption than single-treated samples. All these results indicated that the bio-mediated particulate material based on MICP can provide an effective solution for problematic cases of sandy soil in prevention of bridge scour and road shoulder erosion.

References

ASTM E1845-15, Standard Practice for Calculating Pavement Macrotexture Mean Profile Depth, ASTM International, West Conshohocken, PA, 2015.

ASTM C67-02c, Standard Test Methods for Sampling and Testing Brick and Structural Clay Tile, ASTM International, West Conshohocken, PA, 2002.

ASTM C150 / C150M-18, Standard Specification for Portland Cement, ASTM International, West Conshohocken, PA, 2018.

ASTM D6272-17, Standard Test Method for Flexural Properties of Unreinforced and Reinforced Plastics and Electrical Insulating Materials by Four-Point Bending, ASTM International, West Conshohocken, PA, 2017.

ASTM D6758-18, Standard Test Method for Measuring Stiffness and Apparent Modulus of Soil and Soil-Aggregate In-Place by Electro-Mechanical Method, ASTM International, West Conshohocken, PA, 2018.

ASTM D6951 / D6951M-18, Standard Test Method for Use of the Dynamic Cone Penetrometer in Shallow Pavement Applications, ASTM International, West Conshohocken, PA, 2018.

ASTM D2166 / D2166M-16, Standard Test Method for Unconfined Compressive Strength of Cohesive Soil, ASTM International, West Conshohocken, PA, 2016.

Bu, C., Wen, K., Liu, S., Ogbonnaya, U., & Li, L. (2018a). "Development of bio-cemented constructional materials through microbial induced calcite precipitation." Mater. Struct., 51(1), 30.

Bu, C., Wen, K., Liu, S., Ogbonnaya, U., Dong, Q., Li, L., & Amini, F. (2018b). "Development of a Rigid Full-Contact Mold for Preparing Biobeams through Microbial-Induced Calcite Precipitation." Geotech. Test. J., 42(3).

Bao, R., Li, J., Li, L., Cutright, T.J., Chen, L, Zhu, J. and Tao, J. (2017). "Effect of microbial induced calcite precipitation on surface erosion of granular soils: Proof of concept." Journal of Transportation Research Board, accepted, in print.

Bernardi D, DeJong JT, Montoya BM, Martinez BC (2014) Bio-bricks: biologically cemented sandstone bricks. Constr Build Mater 55:462–469.

Briaud, J. L., Bernhardt, M., & Leclair, M. (2011). The pocket erodometer test: Development and preliminary results. Geotechnical Testing Journal, 35(2), 342-352.

Bentley, W. A. (1904). "Studies of raindrops and raindrop phenomena." Mon Weather Rev 32: 450-456.

Chou, C. W., Seagren, E. A., Aydilek, A. H., & Lai, M. (2011). "Biocalcification of sand through ureolysis." J. Geotech. Geoenviron. Eng., 10.1061/(ASCE)GT. 1943-5606.0000532, 1179-1189.

Consoli, N. C., Vendruscolo, M. A., Fonini, A., & Dalla Rosa, F. (2009). "Fiber reinforcement effects on sand considering a wide cementation range." Geotext. Geomembr., 27(3), 196-203.

Christiansen, J. (1941). "The uniformity of application of water by sprinkler systems." Agricultural Engineering 22(3): 89-92.

DeJong, J. T., Mortensen, B. M., Martinez, B. C., and Nelson, D. C. (2010). "Biomediated soil improvement." Ecology Engineering, 36(2), 197–210.

DeJong, J. T., Fritzges, M. B., & Nüsslein, K. (2006). "Microbially induced cementation to control sand response to undrained shear." J. Geotech. Geoenviron. Eng., 10.1061/(ASCE)1090-0241(2006)132:11(1381), 1381-1392.

Jiang, N. J., Yoshioka, H., Yamamoto, K., & Soga, K. (2016). "Ureolytic activities of a urease-producing bacterium and purified urease enzyme in the anoxic condition: Implication for subseafloor sand production control by microbially induced carbonate precipitation (MICP)." Ecol. Eng., 90, 96-104.

Li, C., Yao, D., Liu, S., Zhou, T., Bai, S., Gao, Y., & Li, L. (2018). "Improvement of geomechanical properties of bio-remediated aeolian sand." Geomicrobiol. J., 35(2), 132-140.

Li, M., Li, L., Ogbonnaya, U., Wen, K., Tian, A., & Amini, F. (2015). “Influence of fiber addition on mechanical properties of MICP-treated sand.” J. Mater. Civ. Eng., 10.1061/(ASCE)MT.1943-5533.0001442, 04015166.

Luk, S.-h., A. D. Abrahams and A. J. Parsons (1993). "Sediment sources and sediment transport by rill flow and interrill flow on a semi-arid piedmont slope, southern Arizona." Catena 20(1-2): 93-111.

Landers, M. N. (1992). “Bridge scour data management.” Hydraulic Engineering: Saving a Threatened Resource-In Search of Solutions: Proceedings of the Hydraulic Engineering Sessions at Water Forum’92, Edited by Jennings, M., and Bhowmik, N. G., American Society of Civil Engineering.

Lagasse, P. F., Clopper, P. E., and Pagán-Ortiz J. E. (2009). Hydraulic Engineering Circular No. 23: Bridge Scour and Stream Instability Countermeasures: Experience, Selection and Design Guidance. Third Edition.

Lagasse, P. F., Clopper, P. E., and Zand evenbergen, L. W (2007). “Countermeasures to protect bridge piers from scour.” NCHRP reports 593, Washington, D.C.

Li, J., and Tao, J. (2015). “Streamlining of bridge piers as scour countermeasure: Optimization of cross section.” Journal of Transportation Research Record, 2521, 160-169.

Moazed, H., A. Bavi, S. Boroomand-Nasab, A. Naseri and M. Albaji (2010). "Effects of climatic and hydraulic parameters on water uniformity coefficient in solid set systems." Journal of Applied Sciences (Faisalabad) 10(16): 1792-1796.

Mortensen, B., M. Haber, J. DeJong, L. Caslake and D. Nelson (2011). "Effects of environmental factors on microbial induced calcium carbonate precipitation." Journal of applied microbiology 111(2): 338-349.

Martinez, B.C., DeJong, J.T., Ginn, T.R., Montoya, B.M., Barkouki, T.H., Hunt C., Tanyu, B., and Major, D. (2013). “Experimental optimization of microbially-induced carbonate precipitation for soil improvement.” Journal of Geotechnical and Geoenvironmental Engineering, 139 (4), 587-598.

Pham, V., Nakano, A., van der Star, W. R. L., Heimovaara, T., & van Paassen, L. (2016). “Applying MICP by denitrification in soils: A process analysis.” Environmental Geotechnics, 5(2), 79-93. [15.00078].

P. Walker, The Australian Earth Building Handbook: HB 195, Standard Australia International Ltd, New South Wales, 2002.

Qabany, A. A., Soga, K., and Santamarina, C. (2012). “Factors affecting efficiency of microbially induced calcite precipitation.” J. Geotech. Geoenviron. Eng, 138(8), 992–1001.

Ramachandran, S. K., V. Ramakrishnan and S. S. Bang (2001). "Remediation of concrete using micro-organisms." ACI Materials Journal-American Concrete Institute 98(1): 3-9.

Stocks-Fischer, S., J. K. Galinat and S. S. Bang (1999). "Microbiological precipitation of CaCO3." Soil Biology and Biochemistry 31(11): 1563-1571.

Shanahan, C., and Montoya, B. M. (2016). “Erosion reduction of coastal sands using microbial induced calcite precipitation.” Geo-Chicago 2016, GSP 269, 42-51.

Shao, W., B. Cetin, Y. Li, J. Li and L. Li (2014). "Experimental investigation of mechanical properties of sands reinforced with discrete randomly distributed fiber." Geotechnical and Geological Engineering 32(4): 901-910.

Whiffin, V. S., van Paassen, L. A., and Harkes, M. P. (2007). “Microbial carbonate precipitation as a soil improvement technique.” Geomicrobiol. J., 24(5), 417–423.

Van Dijk, A., L. Bruijnzeel and C. Rosewell (2002). "Rainfall intensity–kinetic energy relationships: a critical literature appraisal." Journal of Hydrology 261(1-4): 1-23.

Wen, K., Bu, C., Liu, S., Li, Y., & Li, L. (2018a). “Experimental investigation of flexure resistance performance of bio-beams reinforced with discrete randomly distributed fiber and bamboo.” Constr. Build. Mater., 176, 241-249.

Wen, K., Li, Y., Liu, S., Bu, C., & Li, L. (2018b). “Development of an Improved Immersing Method to Enhance Microbial Induced Calcite Precipitation Treated Sandy Soil through Multiple Treatments in Low Cementation Media Concentration.” Geotech. Geol. Eng., 1-13.

Yun, H. D. (2013) Flexural behavior and crack-damage mitigation of plain concrete beam with a strain-hardening cement composite (SHCC) layer at tensile region. Compos B 45(1):377–387.

Zhao, Q., L. Li, C. Li, H. Zhang and F. Amini (2014a). "A full contact flexible mold for preparing samples based on microbial-induced calcite precipitation technology."

Zhao, Q., Li, L, Li, C., Li, M., Amini, F., Zhang, H. (2014b) Factors affecting improvement of engineering properties of MICPtreated soil catalyzed by bacteria and urease. J Mater Civ Eng 26(12):04014094.

Zheng, W., (2013) Instrumentation and Computational Modeling for Evaluation of Bridge Substructures across Waterways. Mississippi Department of Transportation, Report 229.